Taurocholate induces biliary differentiation of liver progenitor cells causing hepatic stellate cell chemotaxis in the Ductular Reaction: Role in pediatric cystic fibrosis liver disease

Pozniak, K. N., Pearen, M. A., Pereira, T. N., Kramer, C. SM., Kalita-De Croft, P., Nawaratna, S. K., Fernandez-Rojo, M. A., Gobert, G. N., Tirnitz-Parker, J. E., Olynyk, J. K., Shepherd, R. W., Lewindon, P. J., & Ramm, G. A.
(2017). Taurocholate induces biliary differentiation of liver progenitor cells causing hepatic stellate cell chemotaxis in the Ductular Reaction: Role in pediatric cystic fibrosis liver disease. *The American journal of pathology*. https://doi.org/10.1016/j.ajpath.2017.08.024

Published in:
The American journal of pathology

Document Version:
Peer reviewed version

Queen's University Belfast - Research Portal:
Link to publication record in Queen's University Belfast Research Portal

Accepted Manuscript

Taurocholate induces biliary differentiation of liver progenitor cells causing hepatic stellate cell chemotaxis in the Ductular Reaction: Role in pediatric cystic fibrosis liver disease.

Katarzyna N. Pozniak, Michael A. Pearen, Tamara N. Pereira, Cynthia SM. Kramer, Priyakshi Kalita-De Croft, Sujeevi K. Nawaratna, Manuel A. Fernandez-Rojo, Geoffrey N. Gobert, Janina EE. Tirnitz-Parker, John K. Olynyk, Ross W. Shepherd, Peter J. Lewindon, Grant A. Ramm

PII: S0002-9440(17)30375-9

DOI: 10.1016/j.ajpath.2017.08.024

Reference: AJPA 2732

To appear in: *The American Journal of Pathology*

Received Date: 6 April 2017

Revised Date: 14 July 2017

Accepted Date: 11 August 2017

Please cite this article as: Pozniak KN, Pearen MA, Pereira TN, Kramer CS, Kalita-De Croft P, Nawaratna SK, Fernandez-Rojo MA, Gobert GN, Tirnitz-Parker JE, Olynyk JK, Shepherd RW, Lewindon PJ, Ramm GA, Taurocholate induces biliary differentiation of liver progenitor cells causing hepatic stellate cell chemotaxis in the Ductular Reaction: Role in pediatric cystic fibrosis liver disease., *The American Journal of Pathology* (2017), doi: 10.1016/j.ajpath.2017.08.024.

Taurocholate induces biliary differentiation of liver progenitor cells causing hepatic stellate cell chemotaxis in the Ductular Reaction: Role in pediatric cystic fibrosis liver disease.

Short title: Taurocholate regulates fibrosis in CF liver disease

Katarzyna N Pozniak[1,2*], Michael A Pearen[1*], Tamara N Pereira[1*], Cynthia SM Kramer[1], Priyakshi Kalita-De Croft[1], Sujeevi K Nawaratna[3], Manuel A Fernandez-Rojo[1,2], Geoffrey N Gobert[3,4], Janina EE Tirnitz-Parker[5,6], John K Olynyk[5,7,8], Ross W Shepherd[1], Peter J Lewindon[1,2,9], and Grant A Ramm[1,2]

*** These authors contributed equally**

Affiliations:

[1] Hepatic Fibrosis Group and [3]Molecular Parasitology Group, QIMR Berghofer Medical Research Institute, Brisbane, QLD, Australia

[2] Faculty of Medicine, The University of Queensland, Brisbane QLD, Australia

[4] School of Biological Sciences, Queen's University Belfast, UK

[5] School of Biomedical Sciences, CHIRI Biosciences, Curtin University, Bentley WA, Australia

[6] School of Medicine and Pharmacology, University of Western Australia, Fremantle WA, Australia

[7] Department of Gastroenterology & Hepatology, Fiona Stanley and Fremantle Hospitals, Perth, WA, Australia

[8] Faculty of Health Sciences, Edith Cowan University, Perth, WA, Australia

[9] Department of Gastroenterology, The University of Queensland, Brisbane, QLD, Australia

Corresponding author:

Prof Grant A. Ramm

Head, Hepatic Fibrosis Group

QIMR Berghofer Medical Research Institute

PO Royal Brisbane and Women's Hospital

Brisbane, Queensland, 4029

Phone: 61-7-33620177

Fax: 61-7-33620191

Email: Grant.Ramm@qimrberghofer.edu.au

Disclosures: The authors have no conflicts of interest and nothing to disclose.

Grant support: This work was supported by a research grant from the National Health and Medical Research Council (NHMRC) of Australia (Grant No. APP1048740 to GAR, PJL, RWS). Professor Grant A. Ramm is supported by a Senior Research Fellowship from the NHMRC of Australia (Grant No. APP1061332). John K. Olynyk is a recipient of a Practitioner Fellowship from the NHMRC of Australia (Grant No. APP1042370).

Number of text pages: 36

Number of figures: 14 + 2 Supplementary figures

Number of Tables: 1

Electronic word count: 3704 (excluding methods, tables/figures, references)

Abstract word count: 220

ABSTRACT

Cystic fibrosis liver disease (CFLD) in children causes progressive fibrosis leading to biliary cirrhosis, however its cause(s) and early pathogenesis are unclear. We hypothesised that a bile acid-induced Ductular Reaction (DR) drives fibrogenesis. We evaluated the DR by cytokeratin-7 immunohistochemistry in liver biopsies, staged for fibrosis, from 60 children with CFLD and demonstrated that the DR was significantly correlated with hepatic fibrosis stage and biliary taurocholate levels. To examine the mechanisms involved in DR induction liver progenitor cells (LPCs) were treated with taurocholate and key events in DR evolution were assessed: LPC proliferation, LPC biliary differentiation and hepatic stellate cell (HSC) chemotaxis. Taurocholate induced a time-dependent increase in LPC proliferation and expression of genes associated with cholangiocyte differentiation (cytokeratin-19, connexin-43, integrin-β4 and γ-glutamyltranspeptidase [GGT]), while the hepatocyte specification marker HNF4α was suppressed. Functional cholangiocyte differentiation was demonstrated via increased acetylated α-tubulin and SOX9 proteins, the number of primary cilia^{+} LPCs and increased active GGT enzyme secretion. Taurocholate induced LPCs to release MCP-1, MIP1α and RANTES into conditioned medium causing HSC chemotaxis, which was inhibited by anti-MIP1α. Immunofluorescence confirmed chemokine expression localized to CK7^{+} DR and LPCs in CFLD liver biopsies. This study suggests that taurocholate is involved in initiating functional LPC biliary differentiation and the development of the DR, with subsequent induction of chemokines that drive HSC recruitment in CFLD.

INTRODUCTION

Cystic fibrosis-associated liver disease (CFLD) is characterized by indolent intrahepatic cholestasis that usually manifests by early adolescence [1]. Cystic fibrosis (CF) is caused by a defect in the gene coding for the cystic fibrosis transmembrane conductance regulator (CFTR) which, among other functions, maintains the flow of bile in contact with cholangiocytes by facilitating the movement of water and bicarbonate ions into bile. Abnormal ion/water transport leads to inspissated bile and cholestasis with focal fibrosing destruction of intrahepatic bile ducts [2]. The resulting pattern of injury is focal biliary cirrhosis for which there is no known treatment and which may progress to cause portal hypertension, multilobular biliary cirrhosis and liver failure. However, only 10% of children with CF will develop portal hypertension and cirrhosis, a higher prevalence than the overall CF population, indicating a strong survival disadvantage. The cause and mechanism of this variable presentation and severity of pathology are not known [3].

The Ductular Reaction (DR) is characterized by the expansion of a population of bipotential liver progenitor cells (LPCs) which can differentiate towards the cholangiocyte lineage into reactive bile ductules, as well as intermediate hepatocytes [4, 5]. LPCs have been proposed by some groups to reside within peri-portal areas associated with the Canals of Hering [6], although their precise cellular origin is the subject of ongoing controversy [7]. LPC expansion is thought to mediate a secondary pathway of liver regeneration, which occurs when the process of hepatocyte replication is overwhelmed in chronic liver disease [8]. In cholestasis this expansion is postulated to be a futile attempt to drain excess bile via the formation of additional bile ductules and to replace damaged hepatocytes [9]. The DR is observed along with activation of hepatic stellate cells (HSCs) and an increase in hepatic fibrosis, which is seen in

adult liver diseases that show periportal damage in cholestatic liver diseases [5, 10], as well as other conditions such as viral hepatitis A [11] and C [12], *HFE*-associated hemochromatosis [13], alcoholic and non-alcoholic fatty liver diseases [14] and post-transplant HCV [15]. This has led to the hypothesis that the two processes of LPC expansion and HSC activation with the resultant DR and fibrosis, respectively, are closely related. While histological evidence of a DR has previously been demonstrated in children with extrahepatic biliary atresia [16, 17], the potential role of LPCs driving HSC activation and fibrosis via development of the DR has not previously been assessed in CFLD.

Bile acids are synthesized in hepatocytes from cholesterol and are usually conjugated to taurine or glycine to form bile salts and secreted into the bile canaliculi. These bile secretions flow into bile ducts, where they are stabilized by bicarbonate ions and water secreted by cholangiocytes as they are excreted from the liver into the gall bladder. They aid lipid digestion in the duodenum by forming micelles. However, their partial hydrophobic nature, which is essential in forming micelles, also makes them toxic to the liver in higher concentrations [18]. The bile salt composition within bile is altered in children with CFLD, as we have previously shown [19], and is comparable to that of mice following bile duct ligation [20]. In particular, the hydrophobic bile salt, taurocholate is significantly increased in both bile and serum of children with CFLD [21]. Taurocholate and other bile salts are able to upregulate the expression of inflammatory genes in the liver [22]. Taurocholate has also been shown to stimulate cytokine secretion from cholangiocytes [23] and hepatocytes [21], which induce transdifferentiation of portal fibroblasts [24] as well as facilitating HSC migration [21, 25]. We previously demonstrated that taurocholate induced the expression of monocyte chemotaxis protein-1 (MCP-1) in normal hepatocytes, and that MCP-1 produced by cholestatic hepatocytes from bile duct-ligated rats induced the chemotaxis of HSCs [21]. Markedly

increased expression of MCP-1 was observed in hepatocytes and cholangiocytes in the liver of children with cholestatic liver diseases [21].

In this study we investigated whether the DR is present in the liver of children with CFLD and examined mechanisms associated with its induction and role in fibrogenesis. We compared the severity of the DR in CFLD liver biopsies with those from other, more aggressively cholestatic pediatric liver disease and then specifically examined a potential mechanism of DR induction in CFLD through investigating the relationship between biliary taurocholate concentrations and the DR in liver biopsies from children with CFLD *in vivo*. We then used *in vitro* cell culture models and *ex vivo* liver slices to investigate the *in vivo* observed effects of elevated taurocholate on LPC differentiation, the secretion of chemokines by LPCs and their chemotactic effects on HSCs in driving hepatic fibrogenesis.

MATERIALS AND METHODS

Patient specimens. This study is part of a long-term prospective cohort study of patients with CFLD identified and referred from the CF Clinic, Royal Children's Hospital, Brisbane, previously well documented [19, 21, 26-28]. CFLD was defined as two of the following: (i) hepatomegaly ± splenomegaly; (ii) persistent (>6mo) elevation of serum alanine aminotransferase (>1.5x upper limit normal); and (iii) abnormal liver ultrasound (abnormal echogenicity or nodular edge). Those with liver synthetic dysfunction or a history of hepatobiliary surgery were excluded. The study conformed to the ethical guidelines of the 1975 Declaration of Helsinki and was approved by the Ethics Committees of the Royal

Children's Hospital, Brisbane and the QIMR Berghofer Medical Research Institute. Informed consent was obtained from parents or patients.

Liver tissue was available from 60 children with CFLD (age, 11.8±4.5yrs). For comparison with other pediatric cholestatic liver diseases, liver tissue was also available from three infants with biliary atresia (BA: age, 1.2±1.4yrs), five with idiopathic neonatal hepatitis (NH: age, 3.4±3.6yrs), as well as four pediatric donor liver controls (age, 6.8±4.5yrs). Bile was available from 7 children with CFLD.

Immunohistochemistry. Formalin-fixed, paraffin-embedded liver sections were subjected to heat antigen retrieval, before exposure to 3% hydrogen peroxide in PBS and Background Sniper (Biocare Medical). Sections were then stained with primary antibody: mouse anti-human CK7 mAb (1:100; DAKO), secondary antibody: rabbit anti-mouse biotinylated IgG (1:400, DAKO), with detection using a streptavidin-biotin/horseradish peroxidase kit (DAKO) and chromogenic substrate 3,3'-diaminobenzidine tetrahydrochloride (Sigma-Aldrich), and counterstained with hematoxylin. Digital images were captured using Aperio ScanScope XT slide scanner (Aperio Technologies) under 20x magnification at 0.5µm/pixel. Image analysis was performed using Aperio Positive Pixel Count algorithm v9.1. Positively stained cells were counted, normalized to the total section area and results correlated with Scheuer's hepatic fibrosis staging.

Biliary taurocholate measurement. Taurocholate concentration was measured in endoscopic bile samples available from seven patients with CFLD, as previously described [21]. Liver biopsies were processed for histochemical CK7 quantification as above. All patients had histological evidence of hepatic fibrosis. Biliary taurocholate levels were correlated with CK7 quantification.

Culture of cell lines and *in vitro* studies. The murine LPC line PIL-2 [29] was cultured in Williams' E medium containing 2mM glutamine, penicillin (100 U/ml), streptomycin (100 µg/ml), insulin (10 µg/ml), epidermal growth factor (10 ng/ml), insulin-like growth factor II (30 ng/ml) and 10% fetal bovine serum (FBS). The human HSC line LX-2 was cultured in DMEM with 2mM glutamine, penicillin (100 U/ml), streptomycin (100 µg/ml) and 2% FBS. PIL-2 cells were treated with taurocholate at 0-300µM concentration to establish a dose-response, with an optimal concentration of 150µM taurocholate chosen for all *in vitro* and *ex vivo* experiments, as previously described [21]. For differentiation assays, cells were lyzed 1-4 days after taurocholate treatment. LPC differentiation was assessed using RT-qPCR and/or western blot analysis evaluating markers for cholangiocyte (connexin 43, *Cx43*; cytokeratin 19, *Ck19*; integrin beta 4, *Itgb4*; γ-glutamyl transpeptidase, *Ggt*; epithelial cell adhesion molecule, *EpCam*; SYR-related HMG box transcription factor 9, *Sox9*) and hepatocyte (albumin; hepatocyte nuclear factor 4α, *Hnf4α*) phenotype.

RT-qPCR for LPC differentiation marker and chemokine mRNA expression. RNA was extracted from both untreated and taurocholate-treated PIL-2 cells using the RNeasy kit (Qiagen) and 1µg was reverse-transcribed into cDNA using SensiFast (Bioline). Real-time qPCR was performed on a Biorad CFX96 with HPRT used as the reference gene. Primers are listed in Table 1.

MTT cell proliferation assay. Cell proliferation was measured over a two hour period at 1-4 days following treatment of PIL-2 cells with 150µM sodium taurocholate using the method of Alley *et al.* [30]. Absorbance was measured at 570nm with a 620nm reference filter.

Western blot analysis.

Cell lysates were prepared from PIL-2 cells disrupted in RIPA buffer with Complete EDTA-free protease inhibitors (Roche). Lysates were resolved on 10% SDS-PAGE gels as described in Laemmli et al. [31] and transferred to polyvinyl difluoride membranes (Immobilon-FL; Millipore). Membranes were probed with anti-CK19 (Abcam ab15463; 1:2000); anti-SOX9 (Merck Millipore #AB5535; 1:1000); anti-HNF4α (Santa Cruz sc6556; 1:1000); anti-acetylated α-tubulin (Sigma-Aldrich T7451; 1:1000); with anti-β-actin used to detect the β-actin loading control (Cell Signaling; 1:2000), in TBST LI-COR Odyssey blocking buffer. Blots were probed with an anti-mouse 680RD or anti-rabbit 800CW secondary at 1:20000 in TBST LI-COR Odyssey blocking buffer. Secondary localization was detected with the LI-COR Odyssey CLx Infrared Imaging System. Band quantification was performed using Image Studio Lite version 5.2.

Immunofluorescence. To examine primary cilia, PIL-2 cells were grown on glass coverslips to 60-80% confluence and treated for three days ± 150μM taurocholate and serum-starved overnight prior to fixation. Cells were placed at 4°C for 30 minutes to destabilize microtubules and then fixed in 4% paraformaldehyde for 10 minutes. Cells were permeabilized with 0.5% Triton X-100, blocked with 5% BSA and probed with mouse anti-acetylated α-tubulin (Sigma-Aldrich; 1:600) and rabbit anti-γ-tubulin (Sigma-Aldrich; 1:400) antibodies overnight in PBST with 1% BSA. Primary binding was probed with AlexaFluor 594 donkey anti-rabbit (Invitrogen) and AlexaFluor 594 goat anti-mouse (Invitrogen) at 1:500 for 1hr in PBST with 1% BSA. Images were captured with a Zeiss AxioScop2. Quantification of acetylated α-tubulin spots was performed using Particle Analysis in ImageJ (NIH).

To identify the cellular source of HSC chemokines in liver biopsies from children with CFLD, we performed dual immunofluorescence for chemokines MCP-1; regulated upon activation, normal T cell expressed and secreted (RANTES); or macrophage inflammatory protein 1α (MIP1α), together with the LPC/DR marker, CK7. Primary antibodies used were: mouse anti-CK7 mAb (1:150, Abcam), goat anti-human MCP-1 pAb (1:8, R&D Systems), goat anti-human CCL5/RANTES pAb (1:83, R&D Systems), goat anti-human MIP1α (1:50, R&D Systems), incubated overnight at 4^{o}C followed by a 30 min incubation step at room temperature with donkey anti-mouse IgG AlexaFluor 555 (1:300, Invitrogen) and donkey anti-goat IgG AlexaFluor 488 (1:300, Molecular Probes). Sections were mounted in Prolong Gold (Invitrogen) with DAPI and examined by confocal microscopy (Zeiss 780NLO).

***Ex vivo* liver slice studies.** Precision-cut liver slices were performed as previously described [32]. A minimum of three liver slices each from three separate C57BL6 WT mice for each time point and each treatment group, were incubated in Williams' E medium containing 2mM glutamine, penicillin (100 U/ml), streptomycin (100 µg/ml) and 10% FBS at 37°C for two and four days ± 150µM taurocholate. Conditioned medium was examined for GGT enzyme activity. Slices were harvested for mRNA quantitation using RT-qPCR.

γ-Glutamyl Transpeptidase Activity Assay. GGT activity was determined from *in vitro* cell cultures and *ex vivo* liver slice conditioned media using the GGT activity colorimetric assay kit (Sigma-Aldrich). Protein for normalization was measured using the Pierce BCA protein assay (Thermo Fisher Scientific).

Quantification of cytokine protein secretion from LPCs ± taurocholate. Chemokines MCP-1, MIP1α and RANTES, released from LPCs, were quantified using the Cytokine Bead

Array (CBD; BD Biosciences), according per manufacturer's protocol. The concentrations of transforming growth factor-1β (TGF-β1) and platelet-derived growth factor–BB (PDGFB) secreted by LPCs were determined by ELISA (R&D Systems).

Chemotaxis assays. Induction of HSC chemotaxis via taurocholate treatment of LPCs was examined by measuring cell migration through 8μm 24-well cell culture inserts (Greiner Bio-One) in modified Boyden chambers. Assays were performed using $0.5x10^6$ LX-2 cells (serum starved overnight) per ml within the insert and the inserts were placed suspended within test medium. Test medium was either normal non-conditioned serum-free Williams' E medium or conditioned medium from LPCs ± taurocholate. Chemokine neutralization was performed by pre-treating conditioned medium with 2.5 μg/ml anti-mouse MCP-1 (AF-479-NA), 1 μg/ml anti-mouse MIP1α (AF-450-NA) or 1 μg/ml anti-mouse RANTES (AF478) polyclonal neutralization antibodies (R&D Systems), 1hr prior to the assay. Testing of MIP1α as chemokine used murine (R&D Systems; 40-337) or human (R&D Systems; 40-364) recombinant purified MIP1α proteins. Blocking of the CCR5 receptor used the neutralization/blocking antibody MAB182 (R&D Systems) applied to the LX-2 cells within the Boyden chamber insert for 1 h prior to the assay at an insert concentration of 20 μg/ml. Chemotaxis assay were performed for 24h and migrated cells on the underside of the insert membrane were stained with Cell Stain (Part No. 90144; Merck-Millipore), treated with Extraction Buffer (Part No. 90145; Merck-Millipore) and absorbance measured at 560nm. Results from separate experimental replicates were normalized to the mean absorbance of control samples (non-conditioned serum-free assay medium and FBS positive control).

Statistical analysis. Results are presented as mean ± SEM. Statistical analysis was performed with GraphPad Prism 6 (GraphPad Software Inc.). For immunohistochemical analysis: Mann-

Whitney test and one-way non-parametric ANOVA analysis with Kruskal-Wallis and Dunn's multiple comparison test. For chemotaxis assay: One-way ANOVA with Sidak's multiple comparison. For qPCR time course: ANOVA with Sidak's post-hoc test and two-way ANOVA to examine the overall treatment effect. For qPCR chemokine expression: unpaired t-test. For CBA assay: unpaired t-test with Welch's correction. Differences were considered significant when $p<0.05$.

RESULTS

Ductular Reaction correlates with fibrosis and biliary taurocholate in CFLD. The DR, as assessed by CK7 expression, was markedly increased in CFLD and contained expanded reactive bile ducts, and both single LPCs and strings of biliary cells/LPCs (**Figure 1**). The DR was mainly present in the periphery of portal tracts as irregular strands/chords of $CK7^+$ cells and as isolated single $CK7^+$ LPCs in adjacent areas. This DR was increased in CFLD ($p<0.05$), as well as in BA ($p=0.114$) and NH ($p=0.016$) versus controls (**Figure 2A**). When stratified for fibrosis stage, there was a highly significant positive correlation between CK7 staining and increasing fibrosis stage in CFLD (Spearman $r = 0.59$, $p < 0.0001$) (**Figure 2B**). Bile samples were available from 7 of the 60 children with CFLD. There was a positive statistical correlation between biliary taurocholate concentrations and the extent of the DR as assessed via CK7 quantification ($r = 0.528$; $p = 0.0321$) (**Figure 2C**).

Taurocholate induces biliary differentiation of LPCs. As we demonstrated that in CFLD the extent of the DR correlates with both fibrosis severity and biliary taurocholate levels, we hypothesized that taurocholate may induce LPC biliary differentiation and the DR. To interrogate this hypothesis, we treated the murine LPC line PIL-2 with 0-300 μM

taurocholate for four days to establish the optimal conditions for all *in vitro* and *ex vivo* studies. Taurocholate induced a dose-dependent increase in mRNA expression of the cholangiocyte markers *Cx43* (**Figure 3A;** ANOVA, p<0.0001) and *Ck19* (**Figure 3B**; ANOVA, p<0.0001). A taurocholate concentration of 150μM was chosen for all subsequent experiments as has previously been described in *in vitro* studies [21, 23], and also being consistent with previous observations in children with CFLD that displayed a mean biliary taurocholate concentration of 108μM vs 41μM in healthy controls [21].

PIL-2 cells were treated with 150μM taurocholate for 0-4 days and markers of cholangiocyte differentiation were further assessed. Taurocholate induced a time-dependent increase in mRNA expression of cholangiocyte markers *Cx43* (**Figure 3C**; ANOVA p<0.0001), *Ck19* (**Figure 3D**; ANOVA p<0.0001), *Itgb4* (**Figure 3E**; ANOVA p<0.029), and *Ggt* (**Figure 3F**; ANOVA p<0.001). Taurocholate treatment did not significantly alter expression of two other cholangiocyte markers, *EpCam* and *Sox9* (data not shown).

Of interest, we observed a concomitant decrease in mRNA expression of the master regulator of hepatic differentiation, *Hnf4α* (**Figure 4A**; ANOVA p=0.0255). A second hepatocyte marker, *albumin (Alb)* showed no significant difference with taurocholate treatment (**Figure 4B**). Taken together, these results suggest that taurocholate augments the cholangiocytic differentiation of the LPC line PIL-2.

LPC proliferation is induced by taurocholate. Integral to the formation of the DR is the expansion of LPCs in chronic liver disease. To assess the potential effect of taurocholate on LPC proliferation, PIL-2 cells ± 150μM taurocholate were subjected to an MTT cell proliferation assay every 24 hrs for 1-4 days. Taurocholate induced a time-dependent increase

in LPC proliferation (**Figure 5**; ANOVA, p=0.0003), which was most notable early, *i.e.*, after 1-2 days.

Taurocholate induces differentiation of LPCs into functional cholangiocytes While Figure 3 demonstrates that taurocholate induced the expression of cholangiocyte-associated genes in LPCs, an assessment of actual cholangiocyte function remained to be confirmed. Thus, we examined expression of proteins involved in various aspects of biliary cell function. We observed that CK19, a protein responsible for the structural integrity of cholangiocytes is significantly induced by taurocholate (**Figure 6A and B**; p=0.0006). Taurocholate also induced a significant >2.5-fold increase in SOX9 protein, a key transcriptional regulator of cholangiocyte differentiation and bile duct formation (**Figures 6A and C**; p=0.001). Conversely, HNF4α protein expression, a marker and transcriptional regulator of hepatocyte specification, was significantly decreased by taurocholate (**Figures 6A and D**; p=0.019).

One key morphological characteristic of cholangiocytes is the presence of primary cilia with acetylated α-tubulin being a key structural component. Western blot analysis revealed a significant induction of acetylated α-tubulin protein expression in taurocholate-treated LPCs (**Figures 6A and E**; p=0.026). As acetylated α-tubulin can also be found within other cellular structures such as microtubule networks, we further investigated the cellular localization of acetylated α-tubulin using immunofluorescence of LPCs ± taurocholate. Expression of acetylated α-tubulin causes primary cilia to appear as discrete dots or lines, while microtubule networks form thin filament-meshed patterns [33]. As can be seen in **Figure 7A**, taurocholate induced a marked increase in the number of acetylated α-tubulin^{+} primary cilia when compared to controls, with quantitation of the relative fluorescence showing a 2.4-fold increase (p=0.022) (**Figure 7B**).

Another measure of functional LPC-cholangiocyte differentiation is the production of enzymatically active GGT, which is expressed and released by cholangiocytes within bile ducts. PIL-2 cells were treated ± 150μM taurocholate for 1-4 days with conditioned medium removed for analysis every 24hrs. Taurocholate induced a significant time-dependent increase in GGT activity (ANOVA, $p<0.0001$), with maximal production between days 3-4 (**Figure 7C**). At the conclusion of the experiment (day 4), this result remained highly significant when corrected for cellular protein concentration (**Supplementary Figure S1**).

The effect of taurocholate in *ex vivo* precision-cut liver slices. To demonstrate potential physiological relevance of our *in vitro* observation, we used precision-cut liver slices from normal control mice, treated ± 150μM taurocholate for up to four days. The hepatic mRNA expression of *Cx43*, as a representative cholangiocyte marker, was significantly increased in a time-dependent manner **(Figure 8A**; ANOVA, $p=0.0354$). Conditioned medium collected was assayed for GGT activity and normalized to liver slice wet weight. Taurocholate again induced a significant increase in GGT activity, peaking at day 2 **(Figure 8B**; ANOVA, $p=0.0021$).

Chemokine expression induced by taurocholate in LPCs. PIL-2 cells treated with 150μM taurocholate showed significantly increased expression of MCP-1, MIP1α, and RANTES mRNA at 6hrs (**Figure 9A**). We also examined the gene expression of the profibrotic cytokine TGF-β1 and HSC mitogen PDGFB, which both have HSC chemotactic potential. While taurocholate induced increased expression of both TGF-β1 and PDGFB, this did not reach statistical significance (**Figure 9A**).

Conditioned medium from PIL-2 cells ± 150μM taurocholate for 6hrs or 24hrs was assessed for protein secretion of key hepatic chemokines. *Rantes*, *Mcp-1*, *Mip1α*, *Tgf-β1* and *Pdgfb* were all expressed constitutively by PIL-2 cells. After 6hrs taurocholate treatment resulted in a 2-fold increase in MIP1α protein release ($p<0.0001$), whereas RANTES and PDGFB increased by approximately 1.5-fold (**Figure 9B**). Taurocholate induced an increase in MCP-1 secretion, however this did not reach statistical significance. By 24hrs, chemokine levels were indistinguishable from controls, except for PDGFB, which remained elevated in response to taurocholate ($p<0.05$). No effect was observed on TGF-β1 release.

HSCs migrate in response to chemokines secreted by taurocholate-treated LPCs. Chemotaxis of the LX-2 HSC line was significantly induced by conditioned medium from PIL-2 cells treated with taurocholate for either 6hrs ($p<0.001$) or 24hrs ($p<0.01$) (**Figure 10A**). Similar levels of chemotaxis were demonstrated using primary rat HSCs (data not shown). To determine the identity of chemokines responsible for this chemotaxis, conditioned medium was pre-treated with neutralizing antibodies to various different chemokines. Chemotaxis was completely inhibited by anti-MIP1α neutralizing antibody (nAb), however, anti-RANTES nAb had no effect (**Figure 10B**). While chemotaxis of LX-2 cells was partially suppressed using anti-MCP-1 nAb, this did not reach statistical significance.

HSCs migrate in response to MIP1α mediated by CCR5. As shown in Fig 10B, chemotaxis of HSCs in response to conditioned medium from PIL-2 cells treated with taurocholate was inhibited by anti-MIP1α nAb. To strengthen the case for the involvement of MIP1α as a HSC chemotactic agent, a chemotaxis assay was performed on LX2 cells using either murine or human recombinant purified MIP1α. Both murine (**Figure 11A;** ANOVA,

p=0.022) and human (**Figure 11B**; ANOVA, p=0.0009) MIP1α produced a significant dose-dependent increase in HSC migration approaching the effect observed with the positive control (FBS).

LX-2 cells were examined for the expression of both known major hepatic MIP1α receptors, C-C chemokine receptor type 1 and 5 (CCR1 and CCR5). Using quantitative RT-PCR, expression of both *Ccr1* and *Ccr5* was demonstrated, with *Ccr5* showing higher mRNA levels vs. *Ccr1* **(Supplementary Figure S2).** To investigate if CCR5 was the major contributing receptor in HSC chemotaxis, LX-2 cells were pre-treated with an anti-CCR5 nAb. This antibody effectively attenuated the migration of LX-2 HSCs in response to both recombinant murine MIP1α **(Figure 11C)** and conditioned medium from PIL-2 cells treated with 150μM taurocholate **(Figure 11D)**.

DR cells and LPCs express chemokines in liver from children with CFLD. To assess the potential clinical relevance of taurocholate-induced chemokine expression demonstrated in *in vitro* and *ex vivo* studies, liver sections from patients with CFLD (n=22) were examined for the cellular source of chemokines. Dual immunofluorescence confirmed that $CK7^+$ DR cells, and single $CK7^+$ LPCs, express MCP-1 (**Figure 12A**), RANTES (**Figure 12B**) and MIP1α (**Figure 13A** and **B**).

DISCUSSION

The DR is proposed to be associated with the initiation of hepatic fibrosis in a number of chronic liver diseases [4, 12, 34, 35]. However, the precise mechanisms involved in its induction and indeed in the interactions between LPCs and HSCs, which may drive both the DR and fibrogenesis, remain to be elucidated. This histological process has been reported in many

adult liver diseases including chronic hepatitis C [12], alcoholic and non-alcoholic steatohepatitis [14, 35] and genetic hemochromatosis [13]. In these diseases, the DR correlates closely with severity of fibrosis and inflammation [34]. However, the presence or role of the DR has not previously been investigated in children with CFLD. Here we show that the DR is indeed present in CFLD (and comparable to the DR present in more aggressive pediatric fibrosing cholestatic diseases such as biliary atresia [36, 37]) and the extent of the DR significantly correlates with fibrosis staging in CFLD, suggesting that mechanisms regulating these two processes are interrelated.

Extensive investigation into the individual mechanisms of LPC and HSC activation [38] have elucidated a role for many different soluble mediators in hepatic fibrosis. Understanding the interaction between LPCs and HSCs is of great importance for clarifying the contribution of these cells in mediating fibrogenesis and for designing therapeutic strategies aimed at reduction of hepatic fibrosis.

Bile salt retention is part of the proposed mechanism of injury and biliary fibrosis in CFLD and we previously demonstrated that biliary/serum levels of the conjugated bile acid taurocholate are elevated in children with CFLD [21]. In the present study we demonstrated that the extent of the DR correlates with biliary taurocholate concentration in children with CFLD and thus speculate a potential mechanistic link. To determine whether taurocholate plays a role in inducing the DR, we used both an LPC *in vitro* cell culture model and *ex vivo* precision-cut liver slices, and employed a reductionist strategy to examine the impact of taurocholate on three key events in the evolution of the DR: LPC proliferation, biliary differentiation of LPCs and HSC chemotaxis.

In this study, we demonstrated that taurocholate increased LPC proliferation *in vitro*, suggesting that taurocholate may play a role in enhancing LPC expansion as part of the DR in CFLD. This observation is supported by studies from Clouzeau-Girard *et al.* [39] showing that taurocholate leads to uncharacterized cell proliferation around the portal tracts in *ex vivo* liver slices. Our data are also consistent with the observation that feeding taurocholate to rats increases cholangiocyte numbers [40], although this study did not distinguish whether these were mature adult cholangiocytes or derived from LPCs.

The biliary differentiation of LPCs and subsequent formation of reactive bile ductular structures appear to be an important component of DR development. We demonstrated a significant increase in expression of the cholangiocyte genes *Ck19, Cx43, Itgb4* and *Ggt1* in response to taurocholate treatment of LPCs. Conversely, the hepatocyte lineage marker *Hnf4α* was decreased, with albumin expression unchanged. This *in vitro* result may be consistent with LPC differentiation that occurs during the DR *in vivo* and provides one potential mechanism for induction of the DR in pediatric cholestatic liver diseases such as CFLD. Further supporting this concept, we demonstrated that taurocholate induced functional cholangiocyte differentiation, evidenced through the increased expression of acetylated α-tubulin, CK19 and SOX9 protein, increased numbers of LPCs elaborating primary cilia, as well as the secretion of enzymatically active GGT *in vitro.* The effect of taurocholate on cholangiocyte function was further confirmed in *ex vivo* precision-cut liver slices, showing induced expression of *Cx43* mRNA and secretion of active GGT.

In addition, this study has demonstrated that taurocholate-exposed LPCs secrete a number of chemokines including MCP-1, MIP1α, RANTES and PDGFB, however HSC chemotaxis in response to taurocholate-treated LPC conditioned medium appears principally due to MIP1α.

Neutralizing antibodies to either MIP1α in LPC conditioned medium or the MIP1α receptor CCR5 on HSCs attenuated TCA-treated LPC-induced HSC chemotaxis. Thus, we propose that MIP1α derived from bile acid-exposed LPCs, may recruit HSCs (via CCR5) during the DR and aid in the initiation of hepatic fibrosis in CFLD. We did not demonstrate that RANTES aided in the chemoattraction of HSCs. Neutralization of MCP-1 resulted in a limited inhibition of HSC chemotaxis, however this did not reach statistical significance due to biological variability of the data. RANTES and MCP-1 may induce recruitment of other cells to the LPC niche as part of the fibrogenic process such as additional LPCs or inflammatory cells, as we previously described [21, 41]. Migration of HSC towards LPCs as well as HSC activation could explain why fibrosis begins in periportal regions of the liver, where there is decreased bile flow through bile ducts, and thus increased accumulation of hydrophobic bile acids [19]. This pattern of chemokine expression upon *in vitro* taurocholate treatment may be indicative of the specific role of LPCs in generating a microenvironment that aids in the activation of HSC. In the current study, immunofluorescence revealed that MCP-1, RANTES and MIP1α are all expressed by DR cells and $CK7^+$ LPCs in liver from children with CFLD, providing *in vivo* evidence validating our *in vitro* observations.

HSC activation is also influenced by other cell types present during chronic liver injury and inflammation, as the LPC niche harbours immune cells including liver macrophages, which also secrete MCP-1, MMPs, TIMPS [42, 43] and chemokines. The downstream chemoattractive effect caused by exposure of LPCs to increased levels of taurocholate appears likely to recruit HSCs into the LPC niche and places these two cell types within close proximity and potentially in direct contact. Supporting this, activated HSCs have been observed adjacent to LPCs in various mouse model of fibrosis [33, 41, 44] as well as in human liver diseases [13, 45], demonstrating recruitment of each cell type towards the other during fibrosis. Various studies

have also suggested that membrane contact (and cross-talk) between LPCs and HSCs is a key mediator of fibrogenesis [41, 46, 47]. In this context, our previous work showed that HSCs treated with the TNF superfamily member, lymphotoxin-β, induces NFκB signalling, upregulating chemotaxis-associated factors such as RANTES and ICAM-1, aiding in LPC and inflammatory cell recruitment. As HSCs express the lymphotoxin-β receptor on their cell surface and lymphotoxin-β is a membrane-bound ligand on LPCs, this suggests that direct cell-cell contact between LPCs and HSCs may be required to initiate chemokine expression [41]. Adding to the complexity of this system, high concentrations of taurocholate have also been shown to induce inflammatory gene expression in hepatocytes as well as cytokine/chemokine secretion that may also lead to HSC recruitment and activation [21, 22]. The present study suggests that the DR precedes fibrosis. However, there is an alternate hypothesis stating that fibrosis precedes the DR and there is some evidence to support this in animal studies [48]. It is also possible that the two processes may be injury context-specific thus further investigations are warranted to fully elucidate the temporal nature of LPC niche development. In addition to HSCs, portal fibroblasts may also contribute to CFLD. However, while previous studies have shown that both activated HSCs and myofibroblasts produce collagen in this disease [26], the role of myofibroblasts derived from portal fibroblasts and indeed the potential recruitment by, and interaction between, these cells and LPCs has not been previously investigated.

In conclusion, this study has shown that the DR is present in CFLD and is correlated with biliary taurocholate levels as well as increasing hepatic fibrosis severity. Thus, we propose that the following model may in part help to explain the pathogenesis of CFLD **(Figure 14)**. In this model, the CFTR defect causes thickened mucous secretions and obstruction of the intrahepatic bile ducts. This obstruction elevates biliary levels of bile salts such as

taurocholate in the vicinity of LPCs, induced as a result of hepatic injury and potentially compromised hepatocyte replication associated with the chronic nature of liver injury in CFLD. In response to supraphysiological levels of bile salts, LPCs firstly undergo proliferation followed by differentiation towards cholangiocytes as part of the DR. Also, in response to altered bile salt levels, LPCs secrete chemokines including MCP-1, MIP1α and RANTES, and this likely attracts HSCs and other immune/inflammatory cells to the LPC niche. Cell-cell contact between LPCs and recruited HSCs may result in activation of HSCs and subsequent fibrogenesis, at least in part via interaction between the HSC lymphotoxin-β receptor via cognate ligands on LPCs, with further inflammatory niche chemotaxis, as we previously described [41]. Increased understanding of the role of hydrophobic bile acids in CFLD and their impact on the LPC niche, cellular cross-talk with HSCs and induction of the DR will provide important new knowledge of clinical relevance, which may aid in the development of targeted therapeutic strategies to reduce fibrosis in CFLD and potentially in other pediatric cholestatic disorders.

ACKNOWLEDGEMENTS:

We would like to thank Clay Winterford, Nigel Waterhouse, Tam Hong Nguyen and Fernando Guimaraes (QIMR Berghofer Medical Research Institute) for technical support and Prof George Yeoh (University of Western Australia) for his kind gift of the PIL-2 murine liver progenitor cell line.

REFERENCES:

[1] Colombo C, Battezzati PM, Crosignani A, Morabito A, Costantini D, Padoan R, Giunta A: Liver disease in cystic fibrosis: A prospective study on incidence, risk factors, and outcome. Hepatology 2002, 36:1374-82.
[2] Lindblad A, Hultcrantz R, Strandvik B: Bile-duct destruction and collagen deposition: a prominent ultrastructural feature of the liver in cystic fibrosis. Hepatology 1992, 16:372-81.
[3] Lindblad A, Glaumann H, Strandvik B: Natural history of liver disease in cystic fibrosis. Hepatology 1999, 30:1151-8.
[4] Roskams TA, Theise ND, Balabaud C, Bhagat G, Bhathal PS, Bioulac-Sage P, Brunt EM, Crawford JM, Crosby HA, Desmet V, Finegold MJ, Geller SA, Gouw AS, Hytiroglou P, Knisely AS, Kojiro M, Lefkowitch JH, Nakanuma Y, Olynyk JK, Park YN, Portmann B, Saxena R, Scheuer PJ, Strain AJ, Thung SN, Wanless IR, West AB: Nomenclature of the finer branches of the biliary tree: canals, ductules, and ductular reactions in human livers. Hepatology 2004, 39:1739-45.
[5] Williams MJ, Clouston AD, Forbes SJ: Links between hepatic fibrosis, ductular reaction, and progenitor cell expansion. Gastroenterology 2014, 146:349-56.
[6] Theise ND, Saxena R, Portmann BC, Thung SN, Yee H, Chiriboga L, Kumar A, Crawford JM: The canals of Hering and hepatic stem cells in humans. Hepatology 1999, 30:1425-33.
[7] Kohn-Gaone J, Gogoi-Tiwari J, Ramm GA, Olynyk JK, Tirnitz-Parker JE: The role of liver progenitor cells during liver regeneration, fibrogenesis, and carcinogenesis. American journal of physiology Gastrointestinal and liver physiology 2016, 310:G143-54.
[8] Lu WY, Bird TG, Boulter L, Tsuchiya A, Cole AM, Hay T, Guest RV, Wojtacha D, Man TY, Mackinnon A, Ridgway RA, Kendall T, Williams MJ, Jamieson T, Raven A, Hay DC, Iredale JP, Clarke AR, Sansom OJ, Forbes SJ: Hepatic progenitor cells of biliary origin with liver repopulation capacity. Nature cell biology 2015.
[9] Burt AD, MacSween RN: Bile duct proliferation--its true significance? Histopathology 1993, 23:599-602.
[10] Desmet VJ: Ductal plates in hepatic ductular reactions. Hypothesis and implications. I. Types of ductular reaction reconsidered. Virchows Archiv : an international journal of pathology 2011, 458:251-9.
[11] Roskams T, van den Oord JJ, De Vos R, Desmet VJ: Neuroendocrine features of reactive bile ductules in cholestatic liver disease. The American journal of pathology 1990, 137:1019-25.
[12] Clouston AD, Powell EE, Walsh MJ, Richardson MM, Demetris AJ, Jonsson JR: Fibrosis correlates with a ductular reaction in hepatitis C: roles of impaired replication, progenitor cells and steatosis. Hepatology 2005, 41:809-18.
[13] Wood MJ, Gadd VL, Powell LW, Ramm GA, Clouston AD: Ductular reaction in hereditary hemochromatosis: the link between hepatocyte senescence and fibrosis progression. Hepatology 2014, 59:848-57.
[14] Roskams T, Yang SQ, Koteish A, Durnez A, DeVos R, Huang X, Achten R, Verslype C, Diehl AM: Oxidative stress and oval cell accumulation in mice and humans with alcoholic and nonalcoholic fatty liver disease. The American journal of pathology 2003, 163:1301-11.
[15] Prakoso E, Tirnitz-Parker JE, Clouston AD, Kayali Z, Lee A, Gan EK, Ramm GA, Kench JG, Bowen DG, Olynyk JK, McCaughan GW, Shackel NA: Analysis of the intrahepatic ductular reaction and progenitor cell responses in hepatitis C virus recurrence after liver transplantation. Liver transplantation : official publication of the American Association for the Study of Liver Diseases and the International Liver Transplantation Society 2014, 20:1508-19.
[16] Fabris L, Cadamuro M, Guido M, Spirli C, Fiorotto R, Colledan M, Torre G, Alberti D, Sonzogni A, Okolicsanyi L, Strazzabosco M: Analysis of liver repair mechanisms in Alagille syndrome and biliary atresia reveals a role for notch signaling. The American journal of pathology 2007, 171:641-53.

[17] Omenetti A, Bass LM, Anders RA, Clemente MG, Francis H, Guy CD, McCall S, Choi SS, Alpini G, Schwarz KB, Diehl AM, Whitington PF: Hedgehog activity, epithelial-mesenchymal transitions, and biliary dysmorphogenesis in biliary atresia. Hepatology 2011, 53:1246-58.
[18] Thomas C, Pellicciari R, Pruzanski M, Auwerx J, Schoonjans K: Targeting bile-acid signalling for metabolic diseases. Nature reviews Drug discovery 2008, 7:678-93.
[19] Smith JL, Lewindon PJ, Hoskins AC, Pereira TN, Setchell KD, O'Connell NC, Shepherd RW, Ramm GA: Endogenous ursodeoxycholic acid and cholic acid in liver disease due to cystic fibrosis. Hepatology 2004, 39:1673-82.
[20] Marschall HU, Wagner M, Bodin K, Zollner G, Fickert P, Gumhold J, Silbert D, Fuchsbichler A, Sjovall J, Trauner M: Fxr(-/-) mice adapt to biliary obstruction by enhanced phase I detoxification and renal elimination of bile acids. Journal of lipid research 2006, 47:582-92.
[21] Ramm GA, Shepherd RW, Hoskins AC, Greco SA, Ney AD, Pereira TN, Bridle KR, Doecke JD, Meikle PJ, Turlin B, Lewindon PJ: Fibrogenesis in pediatric cholestatic liver disease: role of taurocholate and hepatocyte-derived monocyte chemotaxis protein-1 in hepatic stellate cell recruitment. Hepatology 2009, 49:533-44.
[22] Allen K, Jaeschke H, Copple BL: Bile acids induce inflammatory genes in hepatocytes: a novel mechanism of inflammation during obstructive cholestasis. The American journal of pathology 2011, 178:175-86.
[23] Lamireau T, Zoltowska M, Levy E, Yousef I, Rosenbaum J, Tuchweber B, Desmouliere A: Effects of bile acids on biliary epithelial cells: proliferation, cytotoxicity, and cytokine secretion. Life sciences 2003, 72:1401-11.
[24] Kruglov EA, Nathanson RA, Nguyen T, Dranoff JA: Secretion of MCP-1/CCL2 by bile duct epithelia induces myofibroblastic transdifferentiation of portal fibroblasts. American journal of physiology Gastrointestinal and liver physiology 2006, 290:G765-71.
[25] Marra F, Romanelli RG, Giannini C, Failli P, Pastacaldi S, Arrighi MC, Pinzani M, Laffi G, Montalto P, Gentilini P: Monocyte chemotactic protein-1 as a chemoattractant for human hepatic stellate cells. Hepatology 1999, 29:140-8.
[26] Lewindon PJ, Pereira TN, Hoskins AC, Bridle KR, Williamson RM, Shepherd RW, Ramm GA: The role of hepatic stellate cells and transforming growth factor-beta(1) in cystic fibrosis liver disease. The American journal of pathology 2002, 160:1705-15.
[27] Lewindon PJ, Shepherd RW, Walsh MJ, Greer RM, Williamson R, Pereira TN, Frawley K, Bell SC, Smith JL, Ramm GA: Importance of hepatic fibrosis in cystic fibrosis and the predictive value of liver biopsy. Hepatology 2011, 53:193-201.
[28] Pereira TN, Lewindon PJ, Smith JL, Murphy TL, Lincoln DJ, Shepherd RW, Ramm GA: Serum markers of hepatic fibrogenesis in cystic fibrosis liver disease. Journal of hepatology 2004, 41:576-83.
[29] Dumble ML, Croager EJ, Yeoh GC, Quail EA: Generation and characterization of p53 null transformed hepatic progenitor cells: oval cells give rise to hepatocellular carcinoma. Carcinogenesis 2002, 23:435-45.
[30] Alley MC, Scudiero DA, Monks A, Hursey ML, Czerwinski MJ, Fine DL, Abbott BJ, Mayo JG, Shoemaker RH, Boyd MR: Feasibility of drug screening with panels of human tumor cell lines using a microculture tetrazolium assay. Cancer Res 1988, 48:589-601.
[31] Laemmli UK: Cleavage of structural proteins during the assembly of the head of bacteriophage T4. Nature 1970, 227:680-5.
[32] Gobert GN, Nawaratna SK, Harvie M, Ramm GA, McManus DP: An ex vivo model for studying hepatic schistosomiasis and the effect of released protein from dying eggs. PLoS Negl Trop Dis 2015, 9:e0003760.
[33] Grzelak CA, Martelotto LG, Sigglekow ND, Patkunanathan B, Ajami K, Calabro SR, Dwyer BJ, Tirnitz-Parker JE, Watkins DN, Warner FJ, Shackel NA, McCaughan GW: The intrahepatic signalling niche of hedgehog is defined by primary cilia positive cells during chronic liver injury. Journal of hepatology 2014, 60:143-51.

[34] Lowes KN, Brennan BA, Yeoh GC, Olynyk JK: Oval cell numbers in human chronic liver diseases are directly related to disease severity. The American journal of pathology 1999, 154:537-41.
[35] Richardson MM, Jonsson JR, Powell EE, Brunt EM, Neuschwander-Tetri BA, Bhathal PS, Dixon JB, Weltman MD, Tilg H, Moschen AR, Purdie DM, Demetris AJ, Clouston AD: Progressive fibrosis in nonalcoholic steatohepatitis: association with altered regeneration and a ductular reaction. Gastroenterology 2007, 133:80-90.
[36] Hartley JL, Davenport M, Kelly DA: Biliary atresia. Lancet 2009, 374:1704-13.
[37] Gouw AS, Clouston AD, Theise ND: Ductular reactions in human liver: diversity at the interface. Hepatology 2011, 54:1853-63.
[38] Bird TG, Lorenzini S, Forbes SJ: Activation of stem cells in hepatic diseases. Cell and tissue research 2008, 331:283-300.
[39] Clouzeau-Girard H, Guyot C, Combe C, Moronvalle-Halley V, Housset C, Lamireau T, Rosenbaum J, Desmouliere A: Effects of bile acids on biliary epithelial cell proliferation and portal fibroblast activation using rat liver slices. Laboratory investigation; a journal of technical methods and pathology 2006, 86:275-85.
[40] Alpini G, Ueno Y, Glaser SS, Marzioni M, Phinizy JL, Francis H, Lesage G: Bile acid feeding increased proliferative activity and apical bile acid transporter expression in both small and large rat cholangiocytes. Hepatology 2001, 34:868-76.
[41] Ruddell RG, Knight B, Tirnitz-Parker JE, Akhurst B, Summerville L, Subramaniam VN, Olynyk JK, Ramm GA: Lymphotoxin-beta receptor signaling regulates hepatic stellate cell function and wound healing in a murine model of chronic liver injury. Hepatology 2009, 49:227-39.
[42] Duffield JS, Forbes SJ, Constandinou CM, Clay S, Partolina M, Vuthoori S, Wu S, Lang R, Iredale JP: Selective depletion of macrophages reveals distinct, opposing roles during liver injury and repair. The Journal of clinical investigation 2005, 115:56-65.
[43] Olynyk JK, Yeoh GC, Ramm GA, Clarke SL, Hall PM, Britton RS, Bacon BR, Tracy TF: Gadolinium chloride suppresses hepatic oval cell proliferation in rats with biliary obstruction. The American journal of pathology 1998, 152:347-52.
[44] Kohn-Gaone J, Dwyer BJ, Grzelak CA, Miller G, Shackel NA, Ramm GA, McCaughan GW, Elsegood CL, Olynyk JK, Tirnitz-Parker JE: Divergent Inflammatory, Fibrogenic, and Liver Progenitor Cell Dynamics in Two Common Mouse Models of Chronic Liver Injury. The American journal of pathology 2016, 186:1762-74.
[45] Gadd VL, Melino M, Roy S, Horsfall L, O'Rourke P, Williams MR, Irvine KM, Sweet MJ, Jonsson JR, Clouston AD, Powell EE: Portal, but not lobular, macrophages express matrix metalloproteinase-9: association with the ductular reaction and fibrosis in chronic hepatitis C. Liver international : official journal of the International Association for the Study of the Liver 2013, 33:569-79.
[46] Dwyer BJ, Olynyk JK, Ramm GA, Tirnitz-Parker JE: TWEAK and LTbeta Signaling during Chronic Liver Disease. Frontiers in immunology 2014, 5:39.
[47] Tirnitz-Parker JE, Olynyk JK, Ramm GA: Role of TWEAK in coregulating liver progenitor cell and fibrogenic responses. Hepatology 2014, 59:1198-201.
[48] Van Hul NK, Abarca-Quinones J, Sempoux C, Horsmans Y, Leclercq IA: Relation between liver progenitor cell expansion and extracellular matrix deposition in a CDE-induced murine model of chronic liver injury. Hepatology 2009, 49:1625-35.

FIGURE LEGENDS

Figure 1. Evidence of the DR in CFLD. Immunohistochemistry for CK7 expression in the liver of (**A**) a donor control subject (10x magnification; 200µm scale bar) and (**B**, **C**) a child with CFLD. The CFLD patient shows **(B)** a marked DR (8x magnification; 160µm scale bar), and **(C)** numerous single $CK7^+$ LPCs adjacent to areas of DR (40x magnification; 60µm scale bar).

Figure 2. Assessment of the Ductular Reaction in CFLD and other pediatric cholestatic liver diseases. (**A**) CK7 expression in three pediatric cholestatic liver diseases: CFLD, cystic fibrosis liver disease; BA, biliary atresia; NH, idiopathic neonatal hepatitis vs. donor control livers. Statistical calculations were performed using an ANOVA with Kruskal-Wallis test where *$p<0.05$. (**B**) Correlation between CK7 expression and hepatic fibrosis stage in livers of children with CFLD (Spearman $r=0.59$, $p<0.0001$). Statistical calculations were performed using an ANOVA with Kruskal-Wallis test where *$p<0.05$, and **$p<0.01$. (**C**) Correlation between hepatic CK7 expression and biliary taurocholate levels in children with CFLD (n=7; Pearson $r^2=0.528$; one-tailed $p=0.0283$). All data represent mean ± SEM.

Figure 3. Taurocholate induces markers of cholangiocyte differentiation in LPCs. Taurocholate (0-300µM) induced a dose-dependent increase in mRNA expression of cholangiocyte markers (**A**) *Cx43* (ANOVA, $p<0.0001$) and (**B**) *Ck19* (ANOVA, $p<0.0001$) in PIL-2 cells (n=4). Dunnett's multiple comparisons test was performed relative to untreated cells. PIL-2 cells (n=4) treated with 150µM taurocholate for up to 4 days induced a time-dependent increase in the mRNA expression of cholangiocyte markers (**C**) *Cx43* (ANOVA, $p<0.0001$), (**D**) *Ck19* (ANOVA, $p<0.0001$), (**E**) *Itgb4* (ANOVA, $p=0.029$), and (**F**) *Ggt1* (ANOVA, $p=0.001$), expressed relative to vehicle control at each time point. Sidak's multiple

comparisons test was used for comparison at individual time points. All data represented as mean ± SEM and p values are indicated as follows: *p<0.05, **p<0.01, ***p<0.001, and ****p<0.0001.

Figure 4. The effect of taurocholate on markers of hepatocyte differentiation in LPCs. PIL-2 cells treated with 150μM taurocholate for up to 4 days resulted in a time-dependent decrease in mRNA expression for the hepatocyte marker (**A**) Hepatocyte nuclear factor 4α (*Hnf4α*; ANOVA, p=0.0255), expressed relative to vehicle control at each time point, although there was no apparent effect on (**B**) Albumin (*Alb*) expression (n=4). All data represented as mean ± SEM.

Figure 5. LPC proliferation is induced by taurocholate. Taurocholate (150μM) induced a time-dependent increase in cell proliferation (ANOVA, p=0.0003) in PIL-2 cells treated for 0-4 days, as assessed using an MTT assay (n=4). Sidak's multiple comparisons test was performed for treatment comparison at individual time points where **p<0.01. All data represent mean ± SEM.

Figure 6. Taurocholate induces functional characteristics of biliary differentiation in LPCs *in vitro* at the protein level. PIL-2 cells were treated with 150μM taurocholate for 4 days. **(A)** Western blot analysis (n=4) revealed an increased expression of CK19 and SOX9 proteins, while HNF4α protein expression was decreased, relative to the β-actin loading control. Increased expression of acetylated α-tubulin protein relative β-actin was also observed. Band quantification from infrared imaging demonstrated that taurocholate induced statistically significant increases in **(B)** CK19, **(C)** SOX9 and **(E)** acetylated α-tubulin, while conversely, **(D)** HNF4α protein expression was significantly decreased. Data are expressed as

mean ± SEM and statistical significance was assessed using Student's t-test where *p<0.05 and ***p<0.001.

Figure 7. Taurocholate induces morphological and biochemical characteristics of functional biliary differentiation in LPCs *in vitro*. (A) PIL-2 cells (n=3) grown on coverslips were treated with 150μM taurocholate for three days vs untreated controls and serum starved overnight to enhance cilia production. Cells were examined (100x magnification) for the presence of primary cilia via expression of acetylated α-tubulin (green). Cells were also labelled with the nuclear strain (DAPI). These images show an increase in the number of primary cilia in response to taurocholate, which when individually-stained spots/lines of fluorescence were quantified **(B)** show a statistically significant 2.4-fold increase using Student's t-test (n=3) where **p<0.01. Data are expressed as mean ± SEM. **(C)** Taurocholate (150μM, 1-4 days) induced a time-dependent increase in GGT enzyme activity (represented as nmole of p-nitroanilide/hour/ml) in conditioned media from PIL-2 cells (n=4; ANOVA, p<0.0001). Sidak's multiple comparisons test was performed for comparison at individual time points where **p<0.01 and ****p<0.0001. All data represent mean ± SEM.

Figure 8. Effect of taurocholate in an *ex vivo* liver model. To demonstrate the potential physiological relevance of our *in vitro* observation, we used precision-cut liver slices (in triplicate from each of n=3 mice) treated with 150μM taurocholate for 4 days to demonstrate a time-dependent increase in **(A)** mRNA expression of the cholangiocyte marker *Cx43* (ANOVA, p=0.0354), as well as (**B**) GGT enzyme activity normalised to tissue weight (6 replicates from each of n=3 mice; ANOVA, p=0.0021). All data represent mean ± SEM.

Figure 9. Profiling of hepatic chemokines expressed and secreted by LPCs after taurocholate treatment. (**A**) Taurocholate induced a significant increase in *Mcp-1*, *Mip1α,* and *Rantes* mRNA expression in PIL-2 cells at 6 hours. Statistical significance for each gene transcript was assessed using Student's t-test where *p<0.05 and ***p<0.001. (**B**) Taurocholate treatment induced a significant increase in MIP1α and RANTES protein release into the culture medium at 6 hours. MCP-1 and PDGFB were also increased but this did not reach statistical significance. The effect of taurocholate was lost after 24 hours, except for the effect on PDGFB (p=0.0153). TGF-β protein release was not affected by taurocholate treatment. All data represented as mean ± SEM and p values are indicated as follows: *p<0.05 and ***p<0.001.

Figure 10. Treatment of LPCs with taurocholate induces HSC chemotaxis. PIL-2 cells were treated with 150μM taurocholate for 6 hours or 24 hours and conditioned medium (CM) from these cells was used in modified Boyden chambers to examine LX-2 chemotaxis after 24 hours. (**A**) Treatment of LX-2 HSCs with conditioned medium from either 6 or 24 hour taurocholate-treated PIL-2 cells resulted in significant HSC chemotaxis across the Boyden chamber membranes (n>4). (**B**) Chemotaxis of LX-2 cells induced by conditioned medium from 24 hour taurocholate-treated PIL-2 cells was inhibited by anti-MIP1α antibody. Statistical significance was determined using ANOVA with Sidak's multiple comparisons test performed for specific comparisons. All data represent mean ± SEM and p values are indicated as follows: **p<0.01, ***p<0.001, and ****p<0.0001.

Figure 11. MIP1α induces HSC chemotaxis. LX-2 cells were placed in modified Boyden chambers with physiologically relevant concentrations of either **(A)** murine recombinant MIP1α or **(B)** human recombinant MIP1α and assessed for chemotactic potential. MIP1α

produced a significant dose-dependent increase in HSC chemotaxis (ANOVA, p=0.022 and p=0.0009, respectively; n=3). Sidak's multiple comparisons test was performed for treatment comparison where *p<0.05. **(C)** The chemoattractive effect of murine recombinant MIP1α was attenuated by pre-treating LX-2 cells with an anti-CCR5 neutralizing antibody (n=4). **(D)** Pre-treatment of LX-2 cells with anti-CCR5 also attenuated chemotaxis in response to conditioned medium from 24 h taurocholate-treated PIL-2 cells (n=4). ANOVA with Sidak's multiple comparisons test was performed for specific comparisons where **p<0.01 and ****p<0.0001. All data are expressed as mean ± SEM.

Figure 12. Cellular localization of MCP-1 and RANTES expression in liver from children with CFLD. Dual immunofluorescence was performed on CFLD patients to demonstrate the colocalization of $CK7^+$ DR cells with (**A**) MCP-1 protein expression (63x magnification; 20µm scale bar) and (**B**) RANTES protein expression (40x magnification; 50µm scale bar). Sections are shown with DAPI (4',6-diamidino-2-phenylindole) in blue, CK7 in red, and either MCP-1 or RANTES in green, with colocalization (merge).

Figure 13. Cellular localization of MIP1α expression in liver from children with CFLD. Dual immunofluorescence was performed on CFLD patients for the association of MIP1α protein expression with (**A**) clusters of $CK7^+$ DR cells (40x magnification; 1.4 zoom; 20µm scale bar) and (**B**) individual $CK7^+$ LPCs (63x magnification; 20µm scale bar). Sections are shown with DAPI (4',6-diamidino-2-phenylindole) in blue, CK7 in red, and M1Pα in green with colocalization (merge).

Figure 14. **Proposed model for taurocholate-induced DR and fibrogenesis in children with CFLD.** The cystic fibrosis transmembrane conductance regulator (CFTR) defect results

in obstruction of the intrahepatic bile ducts (red cross). This obstruction elevates biliary taurocholate levels, which drives LPC proliferation and biliary/cholangiocyte differentiation as part of the DR. In response to increased taurocholate, LPCs secrete chemokines that attract HSCs/myofibroblasts (and likely other immune/inflammatory cells) to the LPC niche and/or the region of DR development. Cell-cell contact between LPCs and recruited HSCs may result in activation of HSCs and subsequent fibrogenesis.

Table 1: List of qPCR Primers: https://www.ncbi.nlm.nih.gov/nuccore/

Primers	**NCBI accession**	**Forward**	**Reverse**
Tgf-β1	NM_021578	5'-GCTTCAGCTCCACAGAGAAGA-3'	5'-CCAGGCTCCAAATGTAGGGG-3'
Cx43	NM_010288	5'-AGCTAGGCGGCAAAAGTAGG-3'	5'-ACTCACTCATGTATACAGAACCAT-3'
Ck19	NM_008471	5'-GTCGAGGGAGGGGTTAGAGT-3'	5'-CCATCTGAGCTACCAGCGAG-3'
Ggt1	NM_008116	5'-CAGCACCACAGGAAAAGTTGAG-3'	5'-ACGGATTTCACCAGGGACAG-3'
Itgb4	NM_001005608	5'-GACCTATGAAGAAGGTGCTC-3'	5'-GGCTCAGATGCGTGCCATAG-3'
Sox9	NM_011448	5'-AGTACCCGCATCTGCACAAC-3'	5'-TACTTGTAATCGGGGTGGTCT-3'
EpCam	NM_008532	5'-CTGGGAGGAGGATAAAGC-3'	5'-AGAAGAATGGAACAGGGAC-3'
Hprt1	NM_013556	5'-CAAACTTTGCTTTCCCTGGT-3'	5'-TCTGGCCTGTATCCAACACTTC-3'
Rantes	NM_031116	5'-TGCCCACGTGAAGGAGTATTTTTA-3'	5'-TGGCGGTTCCTTCGAGTGACAA-3'
Pdgfb	NM_011057	5'-ATCCGCTCCTTTGATGATCT-3'	5'-GAGCTTTCCAACTCGACTCC-3'
Mip1α	NM_011337	5'-CTGCCCTTGCTGTTCTTCTC-3'	5'-CTTGGACCCAGGTCTCTTTG-3'
Mcp-1	NM_011333	5'-GCTGACCCCAAGAAGGAATG-3'	5'-GTGCTTGAGGTGGTTGTGGA-3'
hCcr1	NM_001295	5'-CCTGCTGACGATTGACAGGTA-3'	5'-TTGGAAAAGTATAAGCCTGGCAT-3'
hCcr5	NM_000579	5'-TGCTACTCGGGAATCCTAAAAACT-3'	5'-TTCTGAACTTCTCCCCGACAAA-3'
Hnf4α	NM_008261	Qiagen QuantiTect cat.no. QT00144739	
Alb	NM_009654	Qiagen QuantiTect cat.no. QT00115570	

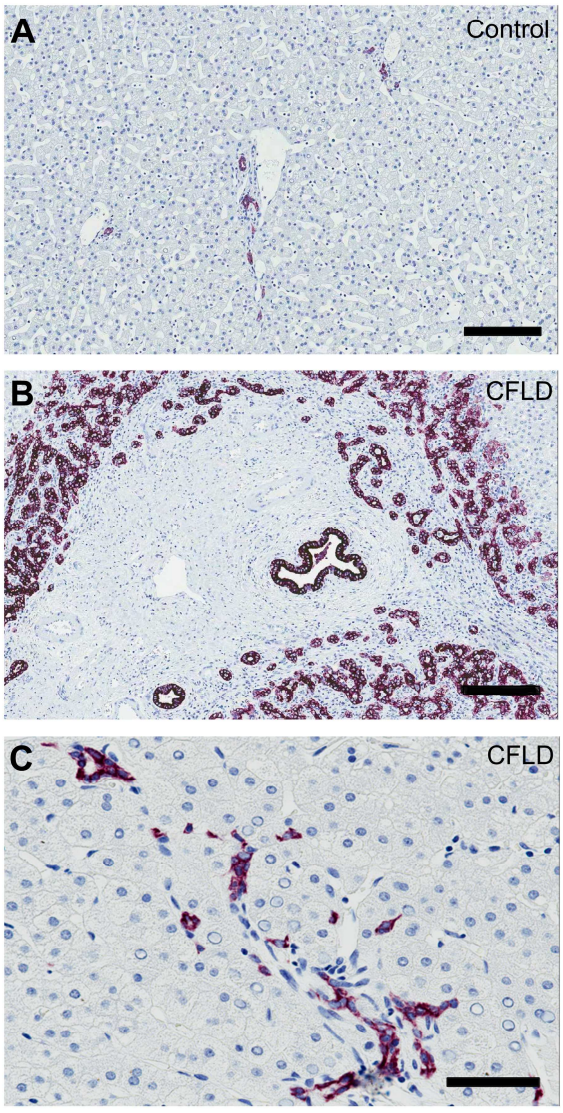
A
Control
B
CFLD
C
CFLD

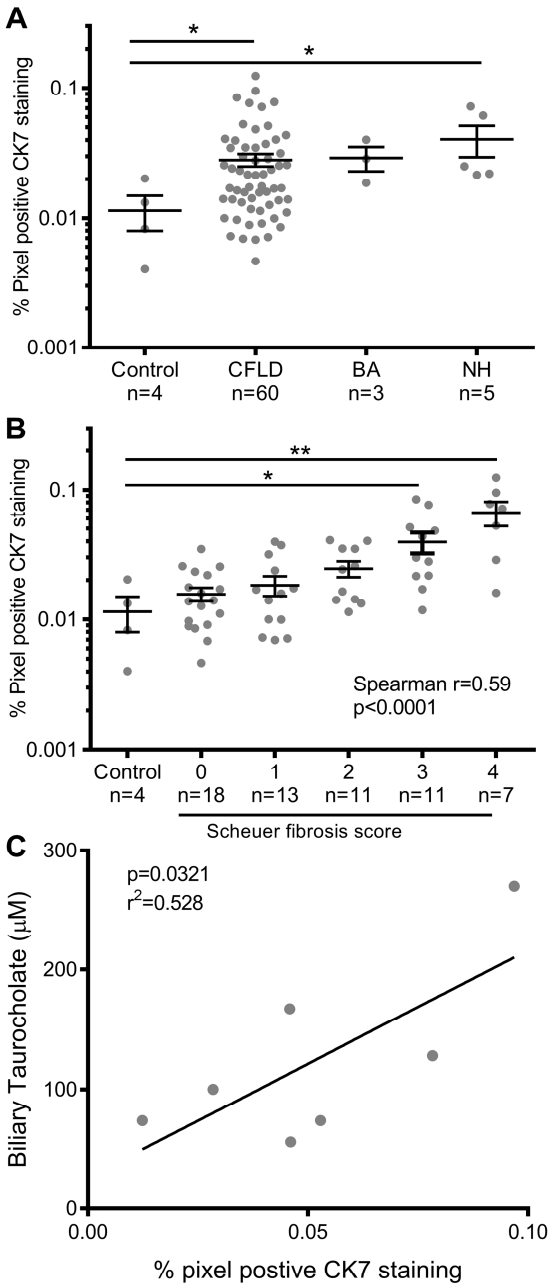
A
*
*
% Pixel positive CK7 staining
0.1
0.01
0.001
Control
n=4
CFLD
n=60
BA
n=3
NH
n=5
B
**
*
% Pixel positive CK7 staining
0.1
0.01
0.001
Spearman r=0.59
p<0.0001
Control
n=4
0
n=18
1
n=13
2
n=11
3
n=11
4
n=7
Scheuer fibrosis score
C
p=0.0321
r2=0.528
Biliary Taurocholate (μM)
300
200
100
0
0.00
0.05
0.10
% pixel postive CK7 staining

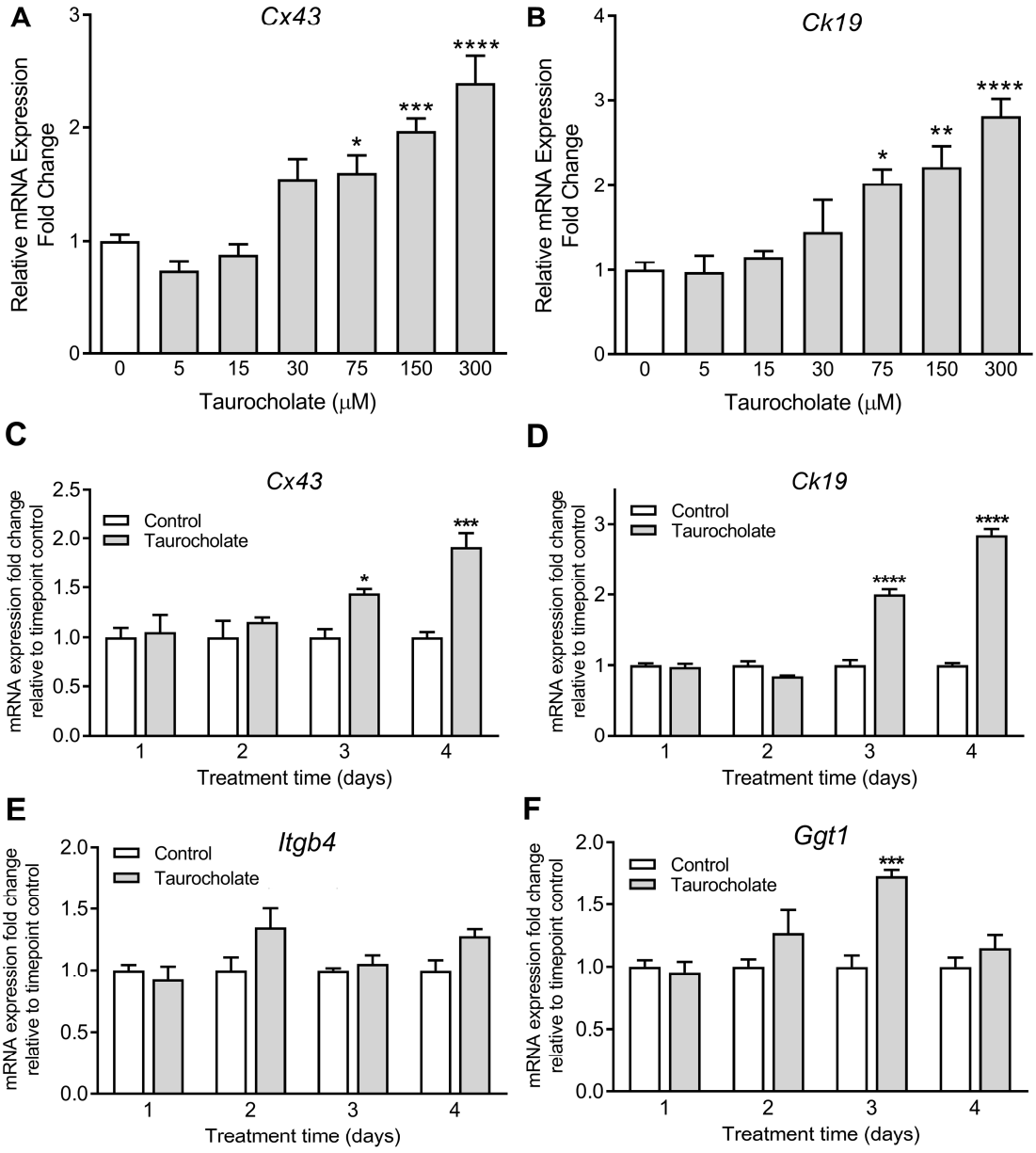
A
Cx43
Relative mRNA Expression
Fold Change
Taurocholate (μM)
0
5
15
30
75
150
300
B
Ck19
Relative mRNA Expression
Fold Change
Taurocholate (μM)
C
Cx43
mRNA expression fold change
relative to timepoint control
Control
Taurocholate
Treatment time (days)
D
Ck19
mRNA expression fold change
relative to timepoint control
Control
Taurocholate
Treatment time (days)
E
Itgb4
mRNA expression fold change
relative to timepoint control
Control
Taurocholate
Treatment time (days)
F
Ggt1
mRNA expression fold change
relative to timepoint control
Control
Taurocholate
Treatment time (days)

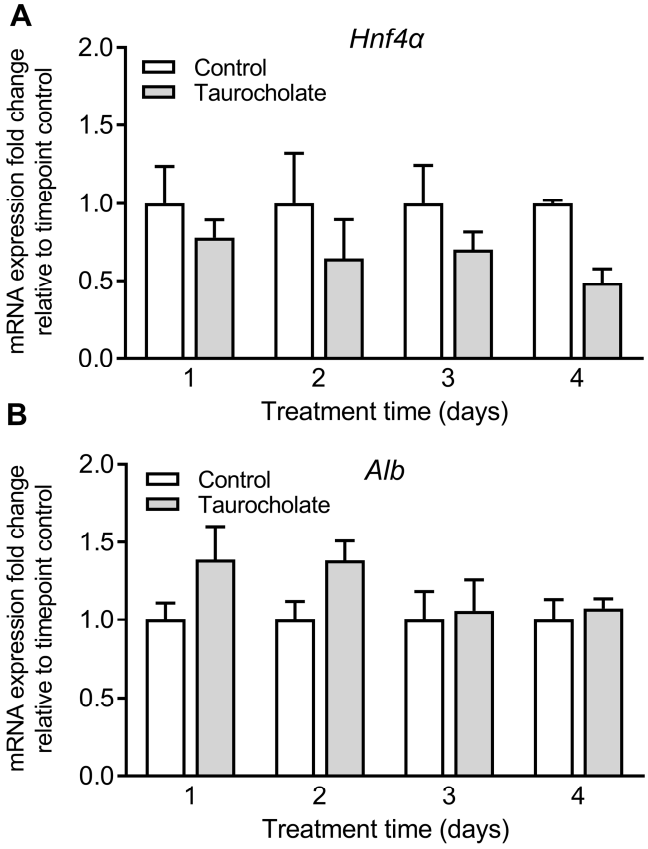
A
Hnf4α
Control
Taurocholate
mRNA expression fold change relative to timepoint control
2.0
1.5
1.0
0.5
0.0
1
2
3
4
Treatment time (days)
B
Alb
Control
Taurocholate
mRNA expression fold change relative to timepoint control
2.0
1.5
1.0
0.5
0.0
1
2
3
4
Treatment time (days)

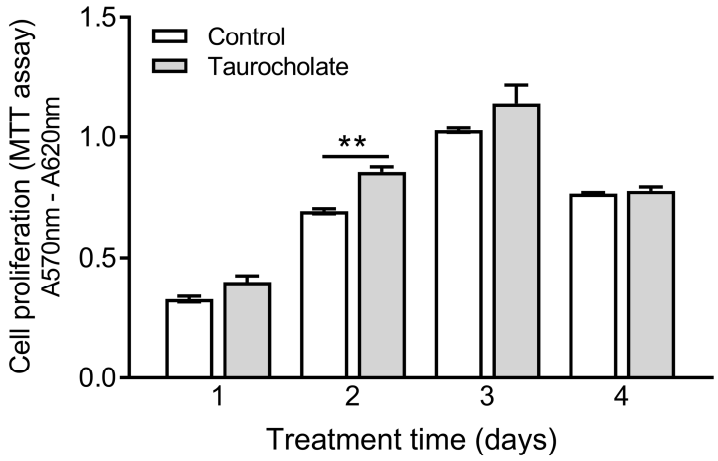
Control
Taurocholate
Cell proliferation (MTT assay)
A570nm - A620nm
1.5
1.0
0.5
0.0
**
1
2
3
4
Treatment time (days)

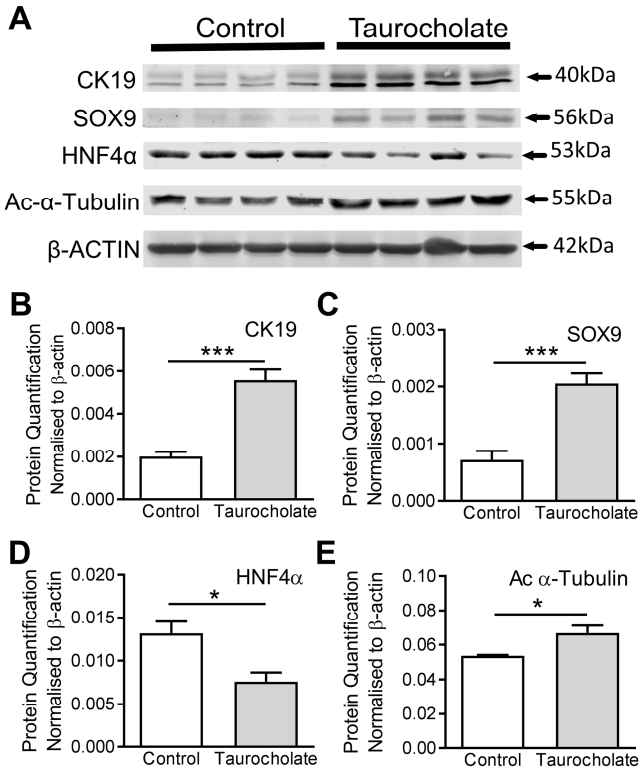
A
Control
Taurocholate
CK19
SOX9
HNF4α
Ac-α-Tubulin
β-ACTIN
40kDa
56kDa
53kDa
55kDa
42kDa
B
CK19
Protein Quantification Normalised to β-actin
0.008
0.006
0.004
0.002
0.000
***
Control
Taurocholate
C
SOX9
Protein Quantification Normalised to β-actin
0.003
0.002
0.001
0.000
***
Control
Taurocholate
D
HNF4α
Protein Quantification Normalised to β-actin
0.020
0.015
0.010
0.005
0.000
*
Control
Taurocholate
E
Ac α-Tubulin
Protein Quantification Normalised to β-actin
0.10
0.08
0.06
0.04
0.02
0.00
*
Control
Taurocholate

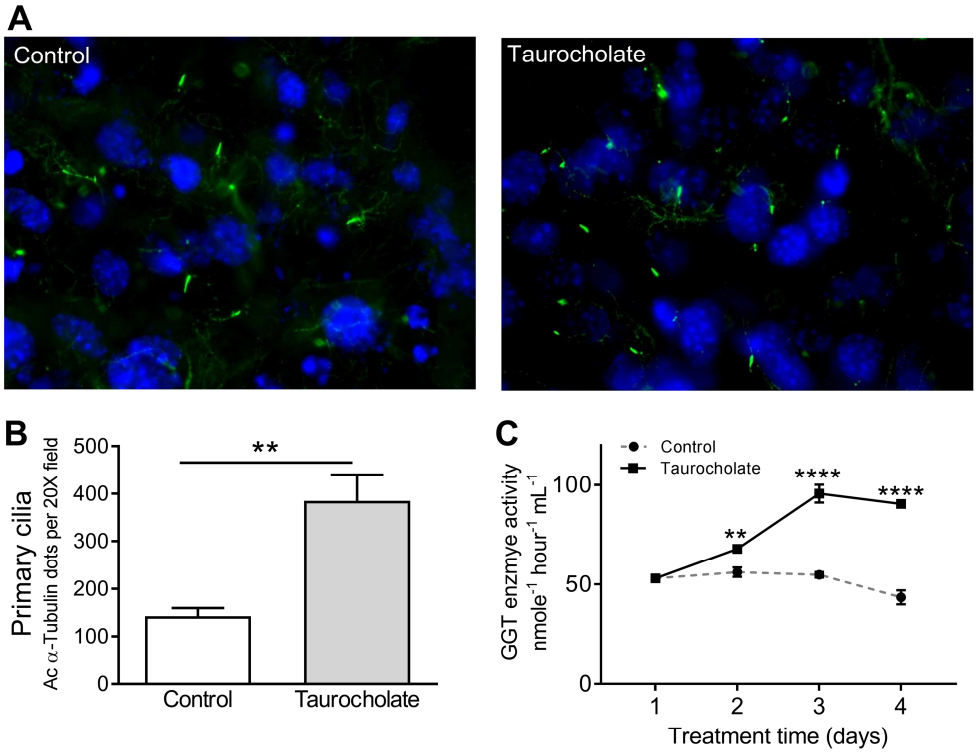
A
Control
Taurocholate
B
Primary cilia
Ac α-Tubulin dots per 20X field
500
400
300
200
100
0
**
Control
Taurocholate
C
Control
Taurocholate
GGT enzmye activity
nmole-1 hour-1 mL-1
100
50
0
**
****
****
1
2
3
4
Treatment time (days)

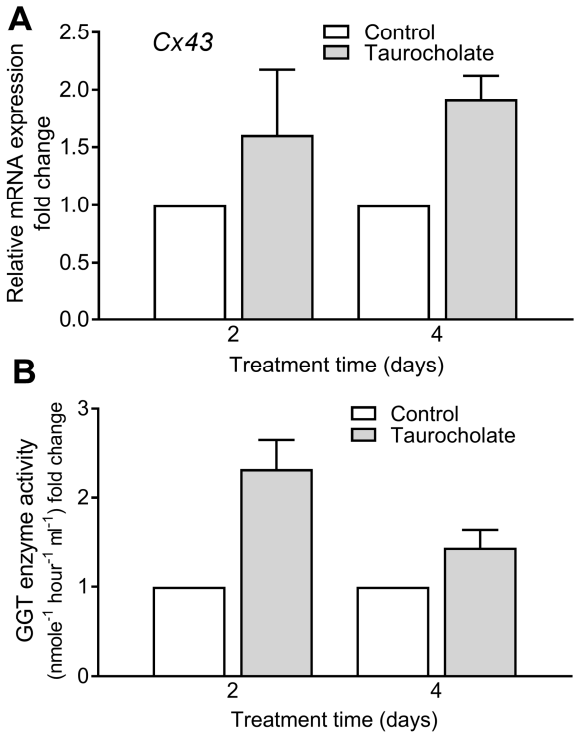
A
Cx43
Control
Taurocholate
Relative mRNA expression
fold change
2.5
2.0
1.5
1.0
0.5
0.0
2
4
Treatment time (days)
B
Control
Taurocholate
GGT enzyme activity
(nmole-1 hour-1 ml-1) fold change
3
2
1
0
2
4
Treatment time (days)

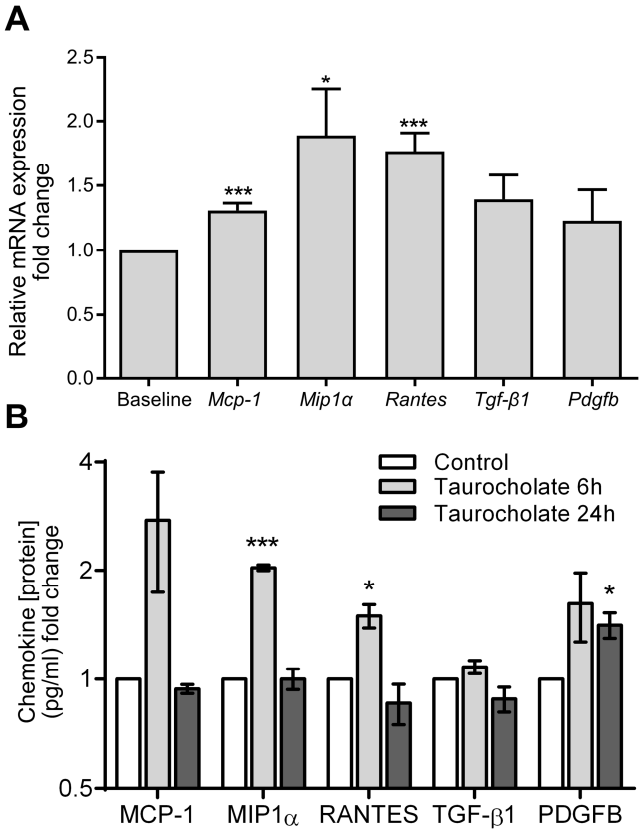
A
Relative mRNA expression fold change
2.5
2.0
1.5
1.0
0.5
0.0
*
***
***
Baseline
Mcp-1
Mip1α
Rantes
Tgf-β1
Pdgfb
B
Chemokine [protein] (pg/ml) fold change
4
2
1
0.5
Control
Taurocholate 6h
Taurocholate 24h
***
*
*
MCP-1
MIP1α
RANTES
TGF-β1
PDGFB

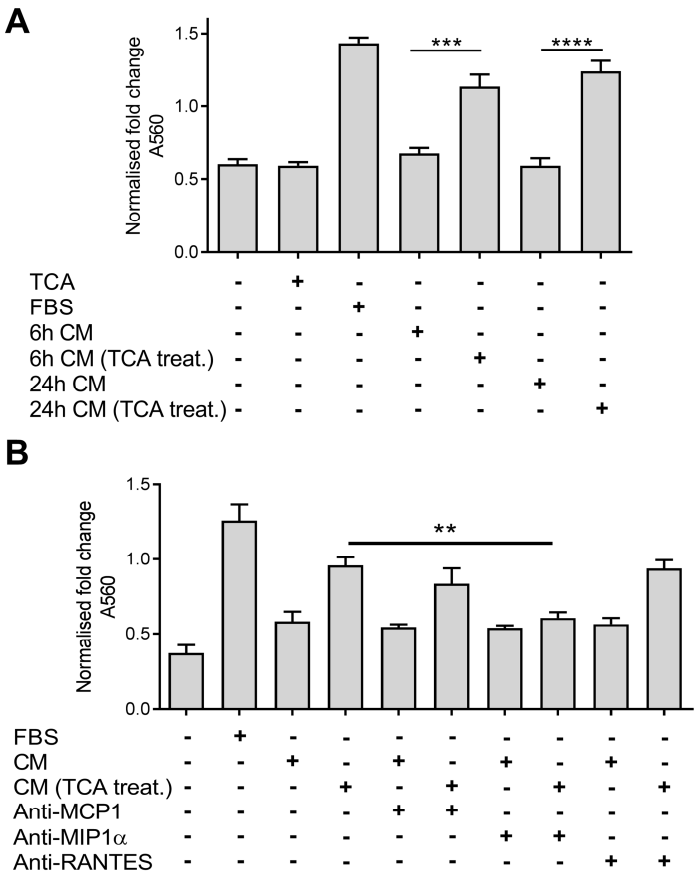
A
Normalised fold change A560
1.5
1.0
0.5
0.0
***
****
TCA - + - - - - -
FBS - - + - - - -
6h CM - - - + - - -
6h CM (TCA treat.) - - - - + - -
24h CM - - - - - + -
24h CM (TCA treat.) - - - - - - +
B
Normalised fold change A560
1.5
1.0
0.5
0.0
**
FBS - + - - - - - - - -
CM - - + - + - + - + -
CM (TCA treat.) - - - + - + - + - +
Anti-MCP1 - - - - + + - - - -
Anti-MIP1α - - - - - - + + - -
Anti-RANTES - - - - - - - - + +

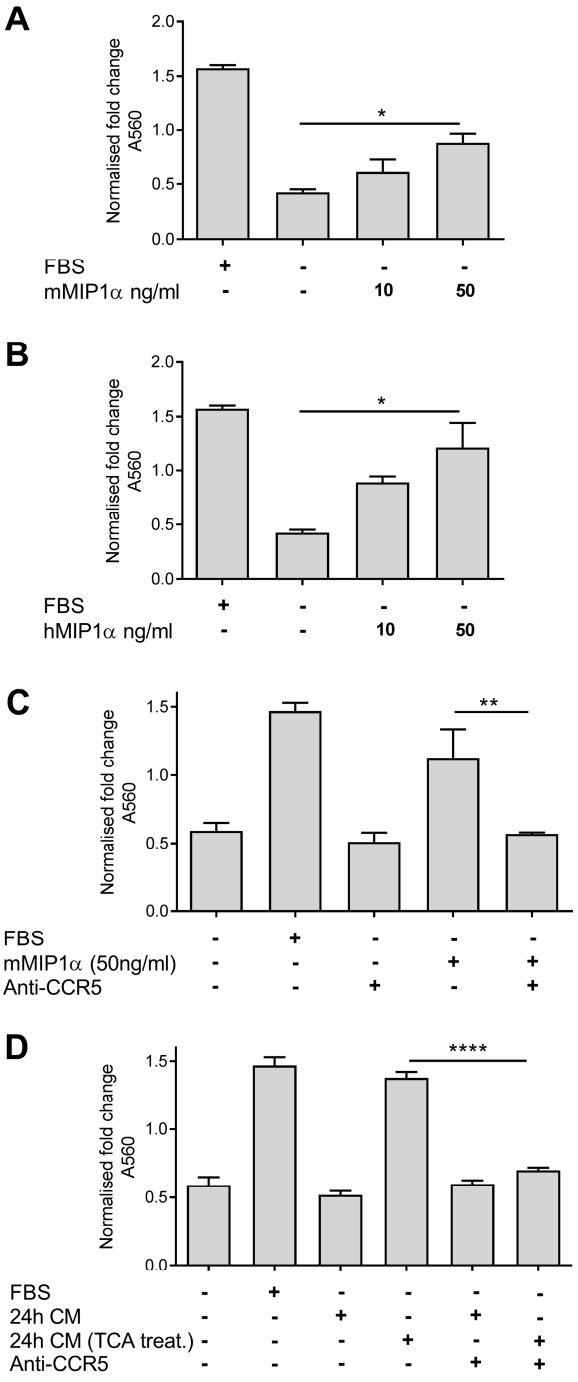
A
Normalised fold change A560
2.0
1.5
1.0
0.5
0.0
*
FBS + - - -
mMIP1α ng/ml - - 10 50
B
Normalised fold change A560
2.0
1.5
1.0
0.5
0.0
*
FBS + - - -
hMIP1α ng/ml - - 10 50
C
Normalised fold change A560
1.5
1.0
0.5
0.0
**
FBS - + - - -
mMIP1α (50ng/ml) - - - + +
Anti-CCR5 - - + - +
D
Normalised fold change A560
1.5
1.0
0.5
0.0
****
FBS - + - - - -
24h CM - - + - + -
24h CM (TCA treat.) - - - + - +
Anti-CCR5 - - - - + +

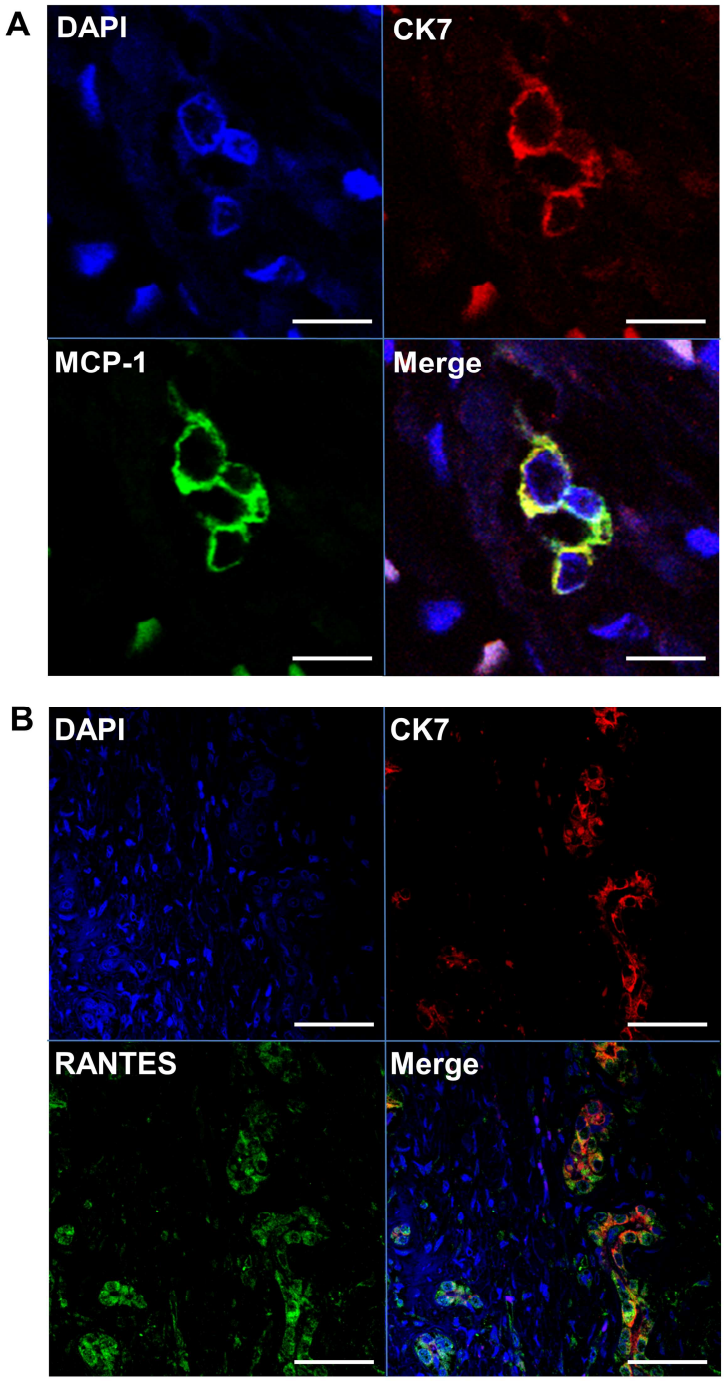
A
DAPI
CK7
MCP-1
Merge
B
DAPI
CK7
RANTES
Merge

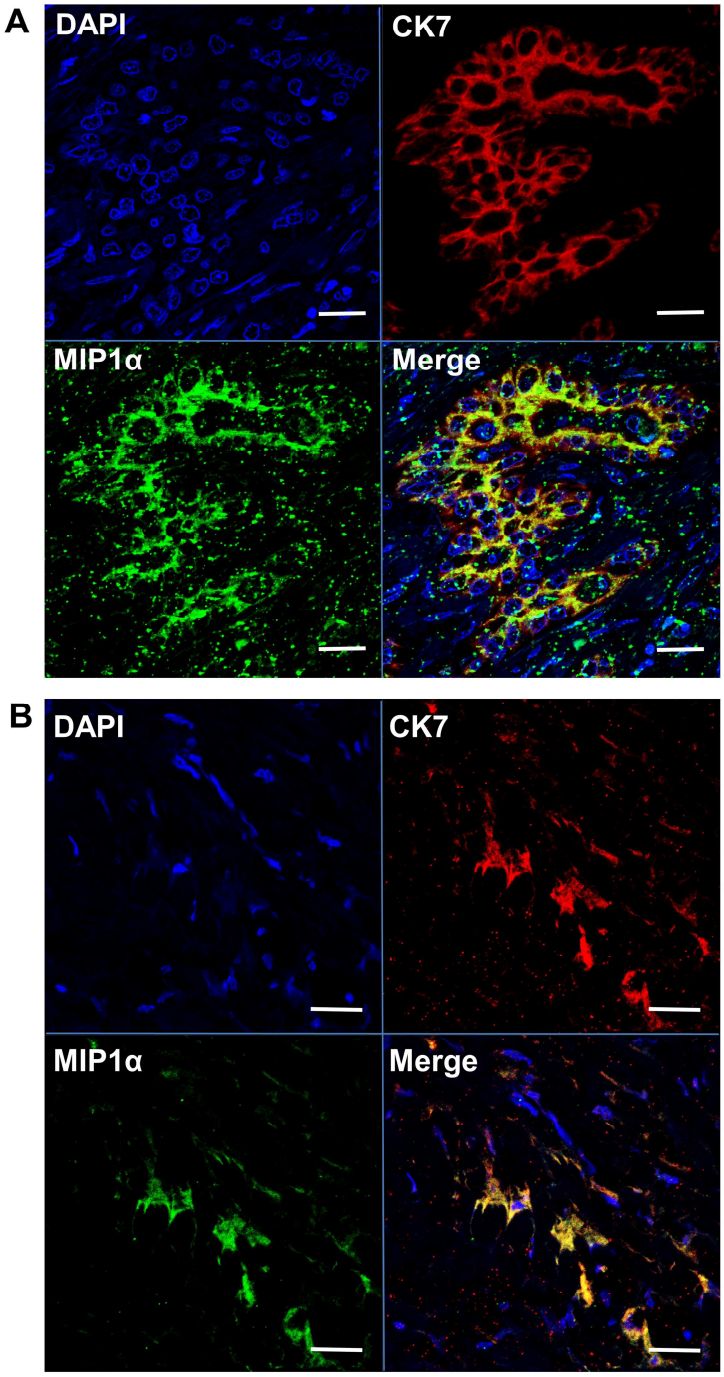
A
DAPI
CK7
MIP1α
Merge
B
DAPI
CK7
MIP1α
Merge

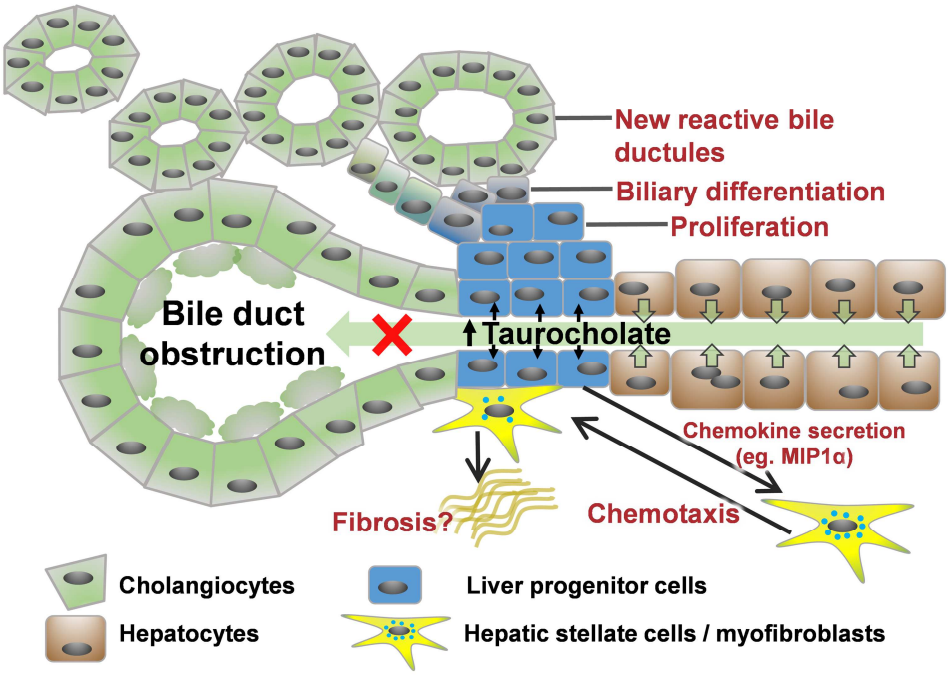
New reactive bile ductules
Biliary differentiation
Proliferation
Bile duct obstruction
Taurocholate
Chemokine secretion (eg. MIP1α)
Fibrosis?
Chemotaxis
Cholangiocytes
Hepatocytes
Liver progenitor cells
Hepatic stellate cells / myofibroblasts

Supplementary Figure Legends

Supplementary Figure 1. GGT enzyme activity in conditioned medium from PIL-2 cells treated ± 150 μM taurocholate (Figure 5D), normalized to protein concentration at the conclusion of the experiment (day 4). Data are expressed as mean ± SEM and statistical significance was assessed using Student's t-test where ***p<0.001.

Supplementary Figure 2. Expression levels of *Ccr1* and *Ccr5*. LX-2 cells were examined for *Ccr1* and *Ccr5* mRNA expression relative to the abundant housekeeping gene *Hprt1*. Data are expressed as mean ± SEM and statistical significance was assessed using Student's t-test where ****p<0.0001.